

Edge effect pinning in superconducting strips with non-uniform distribution of defects

Gregory J. Kimmel,^{1,2} Andreas Glatz,^{1,3} Valerii M. Vinokur,¹ and Ivan A. Sadovskyy^{1,4}

¹*Materials Science Division, Argonne National Laboratory, 9700 S Cass Av, Lemont, IL 60439, USA*

²*Department of Engineering Sciences and Applied Mathematics,
Northwestern University, 633 Clark St, Evanston, IL 60208*

³*Department of Physics, Northern Illinois University, DeKalb, IL 60115, USA*

⁴*Computation Institute, University of Chicago, 5735 S Ellis Av, Chicago, IL 60637, USA*

(Dated: June 15, 2022)

Transport characteristics of nano-sized superconducting strips and bridges are determined by an intricate interplay of surface and bulk pinning. At the same time, they are ideal model systems for comparing experimental, theoretical, and simulation results. In the extremal case of a very narrow bridge, the critical current is mostly defined by its surface barrier, including the contribution from its roughness. On the other hand, the critical current of wide strips is dominated by its bulk properties and mostly determined by the concentration and strength of pinning centers. Here we present a detailed study of the intermediate regime where the critical current is determined, both, by randomly placed pinning centers and by the Bean-Livingston barrier at the edge of the superconducting strip in an external magnetic field. We use the time-dependent Ginzburg-Landau equations to acquire statistics of vortex dynamics and current distribution in the critical regime. We describe the asymmetric case in detail and find that the edge-barrier at the edge, where vortices leave the superconductor, influence the critical current much stronger than the vortex-entrance edge.

Keywords: Type-II superconductivity, critical current, vortex trapping, Bean-Livingston barrier, time-dependent Ginzburg-Landau model

I. INTRODUCTION

Immobilizing magnetic vortices and thus preventing dissipation under applied currents is one of the major objectives for realizing applications of type-II superconductivity.¹⁻⁴ Typically, this vortex pinning is achieved by introducing structural inhomogeneities in the bulk of the material. Recently, it has been recognized that geometric pinning utilizing surface and geometrical barriers for controlling the entrance or exit of vortices in and out of mesoscopic superconductors and superconducting strips can be extremely efficient.⁵⁻¹² Appreciable enhancement of superconducting parameters in strips was recently observed experimentally and explained in terms of surface (edge) superconductivity.^{13,14} One could conclude from these experiments that surfaces may provide one of the most important pinning mechanisms in strips and mesoscopic systems.^{15,16} At the same time, it was observed that the introduction of point-like or cylindrical defects near the surface can be detrimental to the effectiveness of surface barriers^{17,18} since they promote easier vortex penetration across the surface.¹⁹ Hence the effect of structural disorder is two-fold: it arrests the vortex dynamics in the bulk, but ‘contaminates’ surface pinning.²⁰⁻²² Both effects are important in an intermediate width regime where each mechanism is relevant. In the case of narrow strips with widths on the order of the superconducting coherence length, the critical current is mostly defined by its surface barrier and phase slips across the strip are important,^{23,24} while for very wide strips, the critical current is dominated by its bulk pinning properties. This sets the quest for optimizing artificially manufactured disorder in geometrically restricted systems to take advantage of a potentially constructive

interplay of bulk and surface pinning mechanisms.

The present article addresses this problem. To this end, we design an approach allowing us to optimize the concentration and spatial distribution of the bulk point defects in order to achieve the maximum possible critical current taking into account the interplay between the surface barrier blocking penetration of vortices into a superconductor and bulk defects arresting the vortex motion in the interior of the sample. We consider experimentally important systems: superconducting wires having the shape of tapes with widths on the order of a few tens of the superconducting coherence length.³ In order to calculate the critical current for a given arrangement of pins (pinscape), we use a solver for the time-dependent Ginzburg-Landau (TDGL) equation for type-II superconductors.²⁵ This approach describes the vortex dynamics sufficiently well in superconductors near the vicinity of the critical temperature and is capable of reproducing experimental critical currents for a given pinscape.²⁶⁻²⁹

The article is organized as follows. In Sec. II we define the geometry of the superconducting strip, briefly describe the TDGL approach and make preliminary remarks. In Sec. III we present the results of the numerical simulations and discuss them. We summarize our results in Sec. IV.

II. MODEL

We consider a two-dimensional superconducting strip, infinite in the x direction and a finite width W , which is appreciably larger than the superconducting coherence length, ξ , but less than the London penetration depth,

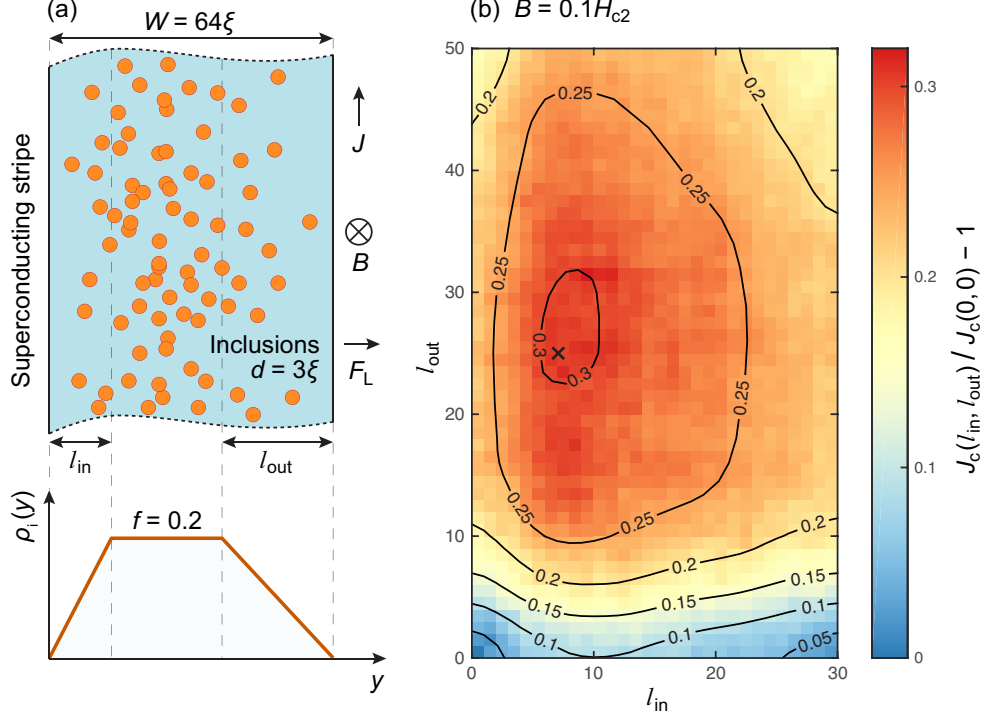


Figure 1. (a) Two-dimensional superconducting strip of width $W = 64\xi$ with non-homogeneous inclusion distribution. The current J is applied vertically (along the x -axis), the magnetic field B is perpendicular to the figure plane, and the resulting Lorentz force F_L acts to the right (along the y -axis). The sample has a length of $L = 1024\xi$ with quasi-periodic boundary conditions in the x direction; in the y direction, we have open boundary conditions, i.e., superconductor-vacuum surfaces. The strip contains (uncorrelated) randomly placed circular inclusions of diameter $d = 3\xi$. The density of these inclusions depends on y : in the middle of the sample, the volume fraction occupied by inclusions is $f = 0.2$, which corresponds approximately to conditions for the maximum possible critical current density in bulk samples. The density of the inclusion $\rho_i(y)$ decreases linearly near the sample boundaries (see bottom plot): within a region of width l_{in} at the boundary where vortices enter the sample and l_{out} at the boundary where vortices leave the sample. (b) The critical current $J_c(l_{in}, l_{out})$ as a function of l_{in} and l_{out} normalized by $J_c(0, 0)$ at applied magnetic field $B = 0.1H_{c2}$. The critical current is increased by $\sim 30\%$ for finite l_{in} and l_{out} compared to the critical current from a homogeneous defect distribution ($l_{in} = l_{out} = 0$). The effect is asymmetric and depends on the direction of vortex motion.

λ . The edges at $y = 0$ and $y = W$ set the positions of the surface barriers. Bulk defects are introduced by spatial modulation of the transition temperature, $T_c(\mathbf{r})$. To evaluate the critical current for the system, we use the

TDGL equation, which simulates the dynamic behavior of the superconducting order parameter $\psi = \psi(\mathbf{r}, t)$:

$$(\partial_t + i\mu)\psi = \epsilon(\mathbf{r})\psi - |\psi|^2\psi + (\nabla - i\mathbf{A})^2\psi + \zeta(\mathbf{r}, t). \quad (1)$$

Here $\mu = \mu(\mathbf{r}, t)$ is the scalar potential, \mathbf{A} is the vector potential generating the external magnetic field $\mathbf{B} = \nabla \times \mathbf{A}$, and $\zeta(\mathbf{r}, t)$ is a temperature-dependent δ -correlated Langevin thermal noise term. The unit of length is defined by the superconducting coherence length $\xi = \xi(T)$ at a given temperature T and the unit of the magnetic field is the upper critical field $H_{c2} = H_{c2}(T)$. Defects in the bulk are realized through the parameter $\epsilon(\mathbf{r}) = [T_c(\mathbf{r}) - T]/[T_{c,\text{bulk}} - T]$, where $T_{c,\text{bulk}}$ is the transition temperature for the clean sample. We solve the TDGL equation in the infinite- λ limit, allowing us to use the gauge $\mathbf{A} = (-B_z, 0, 0)y$ for the vector potential.

We solve Eq. (1) numerically by discretizing the system on a regular grid with mesh size of half a coherence length and integration of time using an implicit massively parallel iterative solver, see Ref. [25] for implementation details. We consider the model system shown in Fig. 1(a), where the two-dimensional superconducting strip lies in the xy plane with quasi-periodic boundary conditions imposed in x direction and open boundary conditions in y direction (i.e., the y component of the current has to obey $J_y = 0$ at these boundaries corresponding to a superconductor-vacuum surface). The magnetic field B is applied in z direction and the external current J is applied in the x direction. In this case, the Lorentz force drives vortices in $+y$ direction (i.e., vortices enter the domain from $y = 0$ and exit at $y = W$).

The current density,

$$\mathbf{J} = \frac{3\sqrt{3}}{2} \left\{ \text{Im}[\psi^*(\nabla - i\mathbf{A})\psi] - \nabla\mu \right\} \quad (2)$$

is measured in units of the depairing current $J_{\text{dp}} = J_{\text{dp}}(T)$.

The magnitude of the critical current in the presence of an external magnetic field is controlled by inclusion patterns, which are small non-superconducting islands immersed in the superconducting matrix. We tune the inclusion size (typically a few ξ) and their spatial distribution. To determine the magnitude of the critical current, we use a finite-electrical-field criterion. Specifically, we chose a certain small external electric field, $E_c = 10^{-4}(3\sqrt{3}/2)J_{\text{dp}}/\sigma$, where σ is the normal conductivity, and adjust the external current, J , to keep this electrical-field criterion on average. The time-averaged value of the external current in the steady state gives the critical current, $J_c = \langle J \rangle$. We start with the two limiting situations: a clean strip and bulk superconductor with defects.

Clean strip. The pinning force in this case is defined by edges at $y = 0$ and $y = W$ with open (no-current) boundary conditions. These boundaries produce the Bean-Livingston barrier^{17,18,30–33} and arrange vortices in ‘rows’ along the current direction.¹⁰ The number of rows depends on the width of the strip W and on the applied magnetic field B . At fixed magnetic field, the most stable configurations are achieved under commensurability conditions. Therefore upon changing the width, the number of the stable rows varies as well, leading to oscillations in

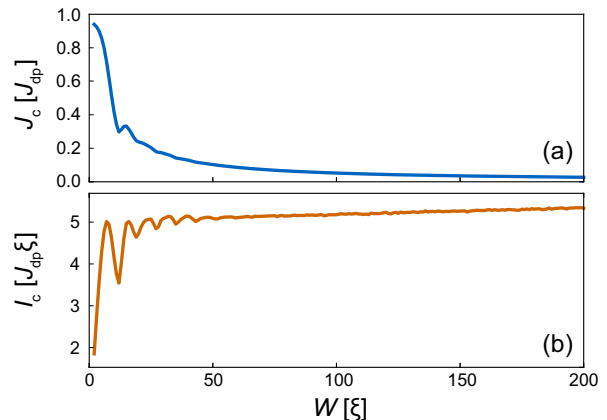


Figure 2. (a) Critical current density J_c and (b) critical current $I_c = J_c W$ as a function of width W of the ideal superconducting strip containing no inclusions in magnetic field $B = 0.1H_{c2}$ applied perpendicular to the strip. The critical current is defined by strip boundaries only and saturates at $I_c \approx 5.1J_{\text{dp}}\xi$ for $W \gtrsim 64\xi$ due to the absence of pinning potentials in the bulk.

the critical current density $J_c(W)$, which are more pronounced in the total critical current $I_c(W) = J_c(W)W$ as shown in Figs. 2(a) and 2(b), respectively. The maxima are realized when the system can accommodate the number of vortices corresponding to the applied field and minima when the system is in between two stable vortex lattice configurations. These oscillations can be best observed for the first few vortex rows. For $W \gg 1$, the critical current I_c saturates at some certain value defined by the depinning forces of the two barriers and depends on the magnetic field.

Bulk superconductor. In this case, the critical current associated with pinning vortices at non-superconducting defects depends on the defect properties (shape, size, concentration) and on the field strength (vortex density). In a three-dimensional (3D) bulk type-II superconductor containing spherical particles and for a wide range of fixed applied magnetic fields, $0.02H_{c2} < B < 0.2H_{c2}$, the optimal critical current is achieved for particle diameters d ranging from 2.5ξ to 4.5ξ and 15–20% volume fraction occupied by particles.³⁴ For large inclusions of fixed diameter $d \geq 3\xi$, the field dependence of the critical current has shown peculiar peaks, associated with the inclusions occupancy by multiple vortices.^{35,36} Similar results are

observed in regular and random pinning configurations of circular (cylindrical) defects in two-dimensional (3D) systems.^{29,37}

General case. Now, we consider geometrically confined 2D systems with circular defects. We design the pinning configuration within our model system with finite W in the following way: (i) the density of the non-superconducting columnar defects far away from the edges is the same as in the bulk case corresponding to the maximum possible critical current; (ii) the density of non-superconducting defects near edges is linearly modulated towards the edges. We define the volume fraction $\rho_i(y)$ occupied by defects of the same diameter d as a function of y which is given by

$$\rho_i(y) = \begin{cases} \frac{y}{l_{\text{in}}} f + \frac{l_{\text{in}} - y}{l_{\text{in}}} f_{\text{in}}, & y < l_{\text{in}} \\ f, & l_{\text{in}} \leq y \leq W - l_{\text{out}} \\ \frac{W - y}{l_{\text{out}}} f + \frac{l_{\text{out}} + y - W}{l_{\text{out}}} f_{\text{out}}, & y > W - l_{\text{out}}. \end{cases} \quad (3)$$

In particular, the volume fraction of the defects changes linearly from f_{in} to its bulk value f at the distance l_{in} from the edge $y = 0$ where vortices enter the sample. On the opposite side of the sample $\rho_i(y)$ changes from f to f_{out} at distance l_{out} .

III. RESULTS AND DISCUSSION

The surface barrier at the superconductor edges prevent vortices, both, from entering and exiting the superconductor. As mentioned in the introduction, non-superconducting defects located at edges or in the vicinity of edges effectively reduce the Bean-Livingston barrier by creating weak spots for vortex penetration.²⁰ We study the interplay between the surface barrier and defect distribution profile $\rho_i(y)$ by investigating the dependence of the critical current density, J_c , on the parameters f , f_{in} , f_{out} , l_{in} , l_{out} , d , in a fixed magnetic field B and fixed sample width $W \gg l_{\text{in}}, l_{\text{out}}$. We numerically solve the optimization problem

$$\mathbf{p}^{\text{opt}} = \arg \max_{\mathbf{p}} J_c(\mathbf{p}) \quad (4)$$

over the six control parameter set $\mathbf{p} = \{f, f_{\text{in}}, f_{\text{out}}, l_{\text{in}}, l_{\text{out}}, d\}$ using a particle swarm optimization routine.³⁷ The resulting optimal parameter set \mathbf{p}^{opt} corresponds to the maximum critical current density $J_c(\mathbf{p}^{\text{opt}})$.

For a wide range of applied magnetic fields, the optimal concentrations of the defects near the entrance and exit boundaries were zero, $f_{\text{in}}^{\text{opt}} = f_{\text{out}}^{\text{opt}} = 0$. This allows us to

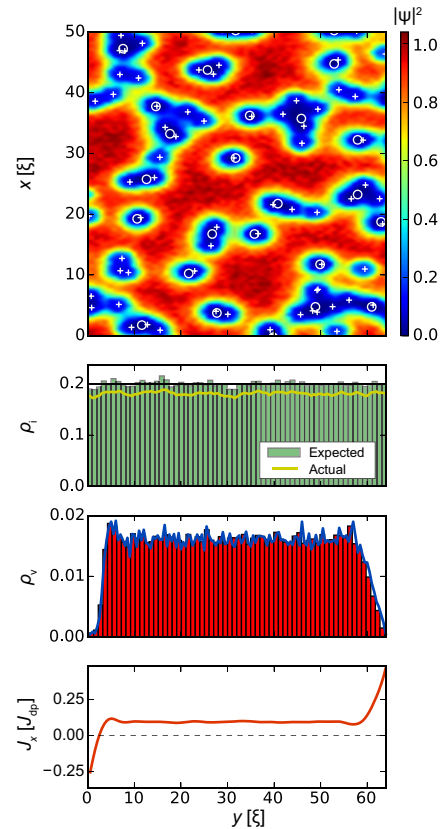


Figure 3. Strip with homogeneous distribution of inclusion density, $l_{\text{in}} = l_{\text{out}} = 0$, $\rho_i = f = 0.2$ in an applied magnetic field $B = 0.1H_{c2}$. *Top panel* shows the squared absolute value of the order parameter $|\psi(\mathbf{r})|^2$. Circles and crosses show inclusion and vortex positions, respectively. *Second panel* shows the distribution of the inclusions across the strip (y direction). The black line shows the ‘requested’ volume fraction $f = 0.2$, the green histogram shows the distribution of the centers of the inclusions, and the yellow line shows the actual volume fraction occupied by the generated defects. (the actual volume fraction is typically lower than the specified/requested one due to defect overlaps and fluctuations of finite random number sequences.) *Third panel* demonstrates the density ρ_v of vortices. *Bottom panel* shows the local current density $J_x(y)$. As expected, the edge screening currents at the surface are in opposite directions, while the small local minimum and maximum a few ξ away from the edge are related to an alignment of vortices at the interior surface barrier. The average critical current density is $J_c^{\text{uniform}} = 0.108J_{\text{dp}}$.

simplify the initial model density profile (3) to

$$\rho_i(y) = \begin{cases} \frac{y}{l_{\text{in}}} f, & y < l_{\text{in}} \\ f, & l_{\text{in}} \leq y \leq W - l_{\text{out}} \\ \frac{W - y}{l_{\text{out}}} f, & y > W - l_{\text{out}}, \end{cases} \quad (5)$$

shown in Fig. 1(a).

The optimal particle diameter d^{opt} decreases with the applied field B and $d^{\text{opt}} \approx 3\xi$ for $B = 0.1H_{c2}$. This result is different from that in the 3D case for spherical

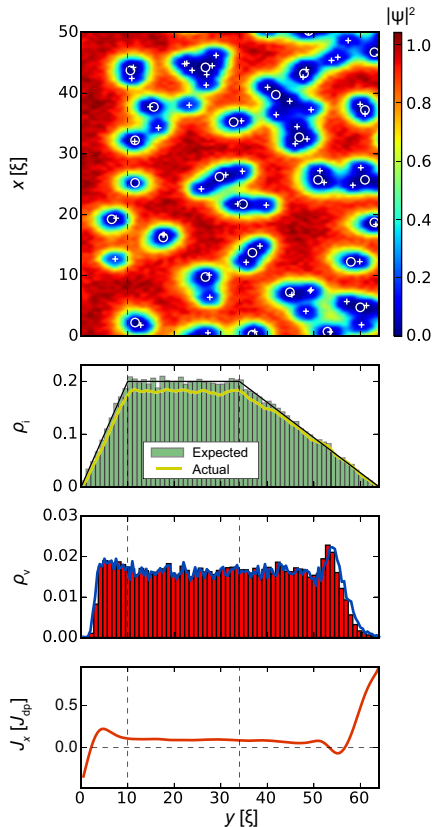


Figure 4. A strip with reduced inclusion density at both edges $l_{\text{in}} = 10\xi$, $l_{\text{out}} = 30\xi$, $f = 0.2$, and $B = 0.1H_{c2}$. The average critical current $J_c^{\text{both}} = 0.14J_{\text{dp}}$ is 28% larger compared to Fig. 3. The $J_x(y)$ dependence has much more pronounced features near the edges. These oscillations in the current are generated by (free) vortex rows in the region of low inclusion density.

particles, which have an optimal diameter of $d^{\text{opt}} \approx 4\xi$ for the same field. This discrepancy in the result is due to the fact that the 2D circular defects we model correspond to columnar defects in 3D samples. It was found earlier that the optimal diameter of columnar defects is smaller than the optimal diameter of spherical defects by approximately one coherence length ξ . Since the optimal volume fraction of defects in both cases is similar,³⁷ around 20%. We stick to $d = 3\xi$ in the following analysis.

Figure 1(b) demonstrates the dependency of the critical current on the distance with reduced defect density at the entrance l_{in} and exit l_{out} of vortices for a sample of width $W = 64\xi$. One can see that the effect is far from symmetric. Figure 1(b) at $B = 0.1H_{c2}$ shows that the critical current has a maximum of $J_c(l_{\text{in}}, l_{\text{out}}) \approx 1.3J_c(0, 0)$ at $l_{\text{in}} \approx 10\xi$ and $l_{\text{out}} \approx 30\xi$. The J_c maximum indicated by a cross was found by a particle swarm optimization routine using l_{in} and l_{out} as optimization parameters. The dependence presented in Fig. 1(b) is a result of the interplay between pinning on inclusions and the Bean-Livingston barrier near the superconducting strip edge.

In the following we will discuss this interplay in detail.

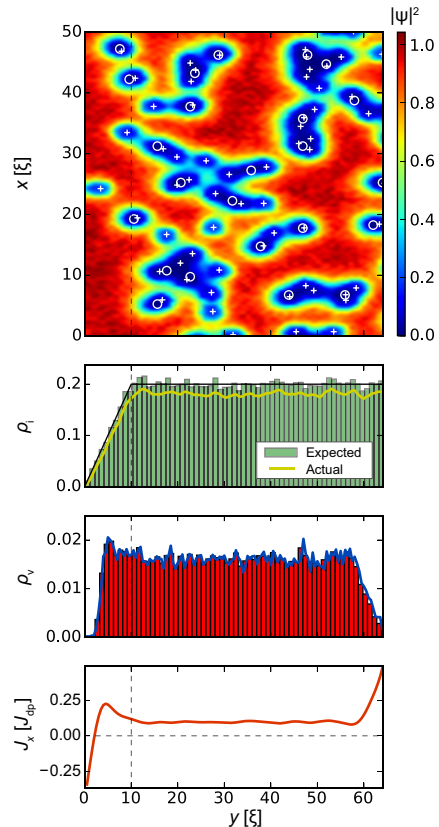


Figure 5. A strip with reduced inclusion density on the entrance side only, $l_{\text{in}} = 10\xi$ and $l_{\text{out}} = 0$, has an average critical current density of $J_c^{\text{in}} = 0.118J_{\text{dp}}$ at applied magnetic field $B = 0.1H_{c2}$.

Our results are summarized in Figs. 3–7. All figures have the same format. *Top panels* show the squared absolute value of the order parameter $|\psi(\mathbf{r})|^2$ in samples of width $W = 64\xi$ (y direction) and length $L = 1024\xi$ (x direction; quasi-periodic boundary conditions). White circles correspond to inclusions, white crosses indicate vortex positions. The presented order parameter configurations are for applied currents $J_x = J_c$. *Second panels* show the distribution of defects along the y direction and averaged over the length of the strip (x direction). The black lines indicate the requested volume fraction $\rho_i(y)$ defined by Eq. (5) with $f = 0.2$ (i.e. 20% of the volume occupied by inclusions in the bulk which corresponds to $B_\Phi/B = 1.78$ inclusions per vortex at $B = 0.1H_{c2}$, where $B_\Phi = 8f/d^2$ is the matching field of the columnar pinning landscape defined by parameters f and d), the green histograms show the distribution of the centers of the inclusions, and the yellow lines show the actual volume fraction occupied by the generated defects. The latter value is somewhat lower than the requested value due to overlapping of inclusions and finite size effects, the real/actual volume fraction can be estimated as $\rho_i^*(y) = 1 - \exp[-\rho_i(y)]$. The requested bulk defect density corresponding to a volume fraction $f = 0.2$ has $f^* \approx 0.181$ real volume fraction. Inclusions overlapping effectively changes the matching

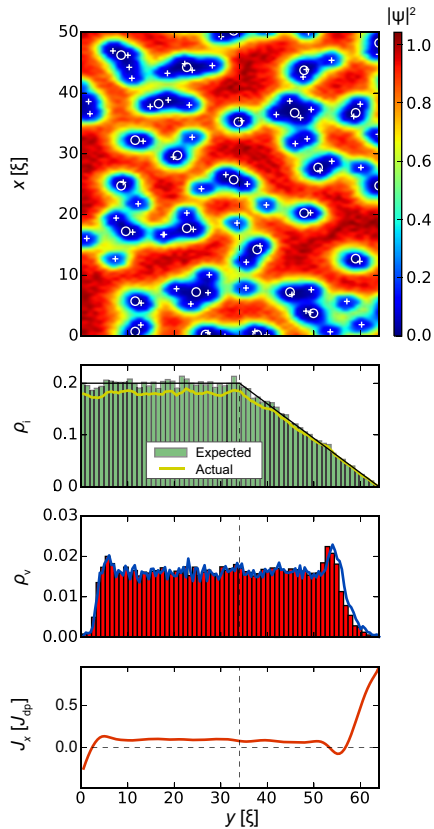


Figure 6. A strip with reduced inclusion density at the exit side only, $l_{\text{in}} = 0$ and $l_{\text{out}} = 30\xi$. The average critical current density is $J_c^{\text{out}} = 0.131J_{\text{dp}}$ at $B = 0.1H_{c2}$.

field to $B_{\Phi}^* = 8f^*/d^2$ and number of inclusions per one vortex to $B_{\Phi}^*/B = 0.161$. *Third panels* demonstrate the density of the vortices $\rho_v(y)$ averaged over the length of the strip. In all cases, the vortex density tends to zero at $y = 0$ and $y = W$ and remains roughly constant in the bulk of the superconductor. *Bottom panels* show the x -component of the local current density, $J_x(y)$, averaged over the length of the strip and are indicative of the edge currents and reflect the distribution of vortices.

Vortex and current density distributions for homogeneous inclusion density $\rho_i = f = 0.2$ for $0 < y < W$ ($l_{\text{in}} = l_{\text{out}} = 0$) are shown in Fig. 3. The position of vortices is strongly correlated with the particular placement of the inclusions, which makes the visual analysis rather complicated. The histograms of defects, vortices, and x -component of current averaged over the sample length L and 10 different realizations of defect distributions contain more useful information. The vortex density is approximately constant in the bulk. This density decreases to zero at $\sim 5\xi$ away from both edges due to the Bean-Livingston barrier. Such a rapid gradient in vortex density produces large surface currents, which has a density on the order of the depairing current density J_{dp} . The average critical current density is $J_c^{\text{uniform}} = 0.108J_{\text{dp}}$.

Figure 4 shows how the result changes when we reduce the inclusion density at both edges of the superconduct-

ing strip. We pick $l_{\text{in}} = 10\xi$, $l_{\text{out}} = 30\xi$, with the remaining volume fraction of inclusions in the bulk as $f = 0.2$ and applied magnetic field $B = 0.1H_{c2}$. The chosen parameters are close to the maximum of $J_c(l_{\text{in}}, l_{\text{out}})$ shown in Fig. 1(b). The critical current $J_c^{\text{both}} = 0.14J_{\text{dp}}$ represents a 30% increase compared to uniform inclusion density J_c^{uniform} . At the same time, the bulk critical current density (for $l_{\text{in}} \lesssim y \lesssim l_{\text{out}}$) remains approximately the same. This indicates that the critical current enhancement is mostly related to the defect distribution near the boundaries of the superconducting strip.

Comparing the vortex configuration in that case with that of the uniform inclusion density case, where the location of vortices is mostly random, we find that this J_c enhancement is produced by the formation of regular vortex row(s) in the regions with a reduced concentration of defects. Each vortex row can be interpreted as an additional potential barrier parallel to the edge repelling vortices. However, since current circulates around each vortex in the row, we can observe the local current flowing in the positive x direction to the right of vortex row and the current flowing in the negative x direction to the left of the vortex row. The value of this local current can be as high as the depairing current density, J_{dp} . This current density can be observed at $y = W$ in Fig. 4. The value of this current is somewhat lower in between rows due to cancellation of opposite screening currents from rows at the left and at the right. Overall, these regular (mostly unpinned) rows lead to oscillations of the average vortex density and subsequently the current density along the applied current direction. This effect is similar to the one observed in artificially manufactured vortex-flow channels in irradiated mesoscopic samples.³⁸

Next we examine how the reduced inclusion density affects the superconducting strip edge where vortices enter and exit the sample separately. The results for the strip with reduced inclusion density at the entrance side only, $l_{\text{in}} = 10\xi$ and $l_{\text{out}} = 0$, is presented in Fig. 5. This pinning landscape generates an average critical current density $J_c^{\text{in}} = 0.118J_{\text{dp}}$. One sees that ‘entrance’ and bulk parts of all histograms, $y \lesssim W/2$, coincides with the corresponding part of Fig. 4 and ‘exit’ and bulk parts $y \gtrsim W/2$ reproduces the same regions in Fig. 3. An analogous situation appears with reduced inclusion density at the exit side of the strip (Fig. 6), $l_{\text{in}} = 0$ and $l_{\text{out}} = 30\xi$. This configuration produces an average critical current density $J_c^{\text{out}} = 0.131J_{\text{dp}}$.

Naturally, values of J_c^{in} and J_c^{out} are in between the two critical current densities of the strip with uniform inclusion distribution and the strip with reduced inclusion density on both edges, i.e., $J_c^{\text{uniform}} < J_c^{\text{in}}, J_c^{\text{out}} < J_c^{\text{both}}$. The independence of the vortex and current configurations on the left and right edges can also be confirmed by comparing differences in the average (or total) critical current of the four configurations discussed above. In particular, $J_c^{\text{both}} + J_c^{\text{uniform}} = J_c^{\text{in}} + J_c^{\text{out}}$ holds for all wide enough strips, $W \gtrsim l_{\text{in}} + l_{\text{out}}$.

Taking into account that (i) the chosen $l_{\text{in}} = 10\xi$ and

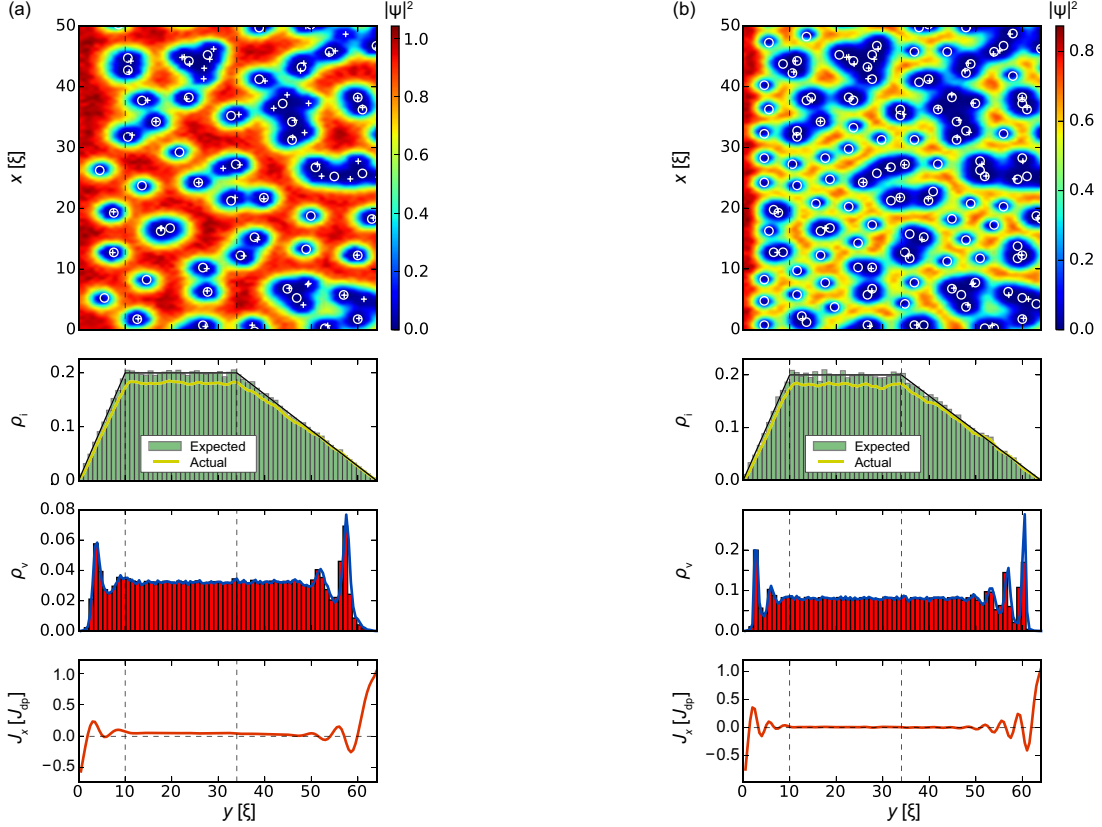


Figure 7. The same as in Fig. 4, but for higher magnetic fields. (a) Field $B = 0.2H_{c2}$ produces an average critical current density $J_c = 0.075J_{dp}$ and (b) field $B = 0.5H_{c2}$ generates $J_c = 0.026J_{dp}$. At higher fields, vortex rows are more dense. This leads to faster oscillations in vortex and local current densities $J_x(y)$. At the exit edge $J_x(y)$ reaches J_{dp} .

$l_{out} = 30\xi$ correspond to the nearly largest critical current at the given magnetic field and (ii) entrance and exit edges act almost independently, we can say that the edge barrier at the entrance can generate additional critical current up to $\delta I_c^{in} = (J_c^{in} - J_c^{uniform})W = 0.51J_{dp}\xi$, while the same addition at the exit edge $\delta I_c^{out} = (J_c^{out} - J_c^{uniform})W = 1.54J_{dp}\xi$ is three times bigger. Note, that the clean strip with ideal boundaries (without any inclusions in the bulk) can generate a total critical current up to $I_c \approx 5.1J_{dp}\xi$ at the same applied magnetic field, see Fig. 2(b).

Higher magnetic fields decreases the distance between neighboring vortex rows and thus leads to higher frequency oscillations of vortex density and the x -component of current in regions with reduced inclusion density as shown in Fig. 7. A magnetic field $B = 0.2H_{c2}$ corresponds to a critical current density $J_c = 0.075J_{dp}$ [Fig. 7(a)] and field $B = 0.5H_{c2}$ to $J_c = 0.026J_{dp}$ [Fig. 7(b)]. On the exit side, the current density $J_x(W)$ reaches the depairing current density J_{dp} .

type	f^{opt}	l_{in}^{opt}	l_{out}^{opt}	J_c^{opt}/J_{dp}	cf. C
C	0.0	-	-	0.080	100%
U	0.2	0	0	0.108	135%
I	0.2	10ξ	0	0.118	148%
O	0.2	0	30ξ	0.131	164%
IO	0.2	9ξ	31ξ	0.142	178%

Table I. Highest critical currents in a strip of width $W = 64\xi$ at $B = 0.1H_{c2}$ for different defect distributions and their optimal configurations: C – Clean strip, U – Uniform defect distribution, I n – Eq. (5) with $l_{out} = 0$, O ut – Eq. (5) with $l_{in} = 0$, and IO – Eq. (5). The defects are circular with diameter $d = 3\xi$.

IV. CONCLUSIONS

In this article we studied the interplay of surface potential barrier and bulk pinning centers in mesoscopic superconducting strips, where both pinning mechanisms are relevant. Fig. 2 suggests that the critical current reaches saturation at $W \sim 64\xi$ in a clean strip, meaning that the effect of the surface barriers on I_c starts to decrease above that width and bulk defects become the dominant pinning mechanism. Since non-superconducting defects are

detrimental for the Bean-Livingston barrier, we studied the general case of a non-homogeneous defect distribution across the width of the strip to be able to take advantage of both mechanisms. In particular, we assumed a linear modulation of the defect concentration near both edges of the strip. This allowed us to quantify the suppression of the surface barrier by defects in the vicinity of the strip edges by studying the vortex and supercurrent distribution in these regions.

Table I summarizes the results for our benchmark system — a strip of width 64ξ in a magnetic field $B = 0.1H_{c2}$: The clean strip (labeled C) has a critical current density of $0.080J_{dp}$, which decreases as $\sim W^{-1}$ for increasing strip width, see Fig. 2. Adding a homogeneous uniform defect density to this system (U) increases the J_c by 35%, which means that the bulk pinning is more relevant than the suppression of the surface barrier. We can expect that J_c would actually decrease for more narrow strips and will reach the bulk critical current value for $W \rightarrow \infty$. In order to extract more detailed information about the suppression of the Bean-Livingston barrier, we introduced the linear defect modulation near the edges. Studying first the vortex entrance and exit edges independently, we first found that defects have a non-symmetric effect on either side of the strip. A linear increase of the defect density at the entrance edge (I) over 10ξ increases the critical current density by another 9% compared to U, while a density decrease at the exit edge (O) over 30ξ adds 21% to J_c compared to U. At the same time, this side is more sensitive to the contamination by defects located at some distance to the surface. For larger W we can expect that the effect of the defect

modulation near the edges on J_c decreases. Both widths, l_{in} and l_{out} , in those two cases are optimal, i.e., lead to the biggest increase of J_c .

Finally, for defect density modulations at both edges (IO), Eq. (5), one obtains an increase of 31% over the U system for optimal values 9ξ and 31ξ for l_{in} and l_{out} , respectively, i.e., the effects from both sides of the strip add up independently. Compared to the clean strip this is a J_c -increase of 78%. One can expect that those optimal values for l_{in} and l_{out} remain independent of W for wider strips. Again, their overall influence on wider strips diminishes as the edges are local. The situation for more narrow strips becomes more complex, in particular when $W \lesssim l_{in}^{opt}(W = 64\xi) + l_{out}^{opt}(W = 64\xi)$. The bulk region with constant defect density vanishes at this point and eventually all defects need to disappear in very narrow strips to get the largest critical current.

Overall, a non-homogeneous defect density demodulation can significantly improve the critical current in mesoscopic superconducting strips.

Acknowledgments. We are delighted to thank A. E. Koshelev and R. Willa for illuminating discussions. The research was supported by the Scientific Discovery through Advanced Computing (SciDAC) program funded by U.S. Department of Energy Office of Science, Advanced Scientific Computing Research. Simulations were performed at [Oak Ridge LCF](#) supported by DOE under contract DE-AC05-00OR22725, at [Argonne LCF](#) (DOE contract DE-AC02-06CH11357), and [Computing Facility](#) at Northern Illinois University. Other simulations using time-dependent Ginzburg-Landau model can be found at [OSCon website](#) and [YouTube channel](#).

-
- ¹ G. Blatter, M. V. Feigel'man, V. B. Geshkenbein, A. I. Larkin, and V. M. Vinokur, *Rev. Mod. Phys.* **66**, 1125 (1994).
- ² T. G. Holesinger, L. Civale, B. Maiorov, D. M. Feldmann, J. Y. Coulter, D. J. Miller, V. A. Maroni, Z. Chen, D. C. Larbalestier, R. Feenstra, X. Li, Y. Huang, T. Kodanandath, W. Zhang, M. Rupich, and A. Malozemoff, *Adv. Mater.* **20**, 391 (2008).
- ³ A. P. Malozemoff, *Annu. Rev. Mater. Res.* **42**, 373 (2012).
- ⁴ W.-K. Kwok, U. Welp, A. Glatz, A. E. Koshelev, K. J. Kihlstrom, and G. W. Crabtree, *Rep. Prog. Phys.* **79**, 116501 (2016).
- ⁵ G. Stan, S. B. Field, and J. M. Martinis, *Phys. Rev. Lett.* **92**, 097003 (2004).
- ⁶ E. Zeldov, A. I. Larkin, V. B. Geshkenbein, M. Konczykowski, D. Majer, B. Khaykovich, V. M. Vinokur, and H. Shtrikman, *Phys. Rev. Lett.* **73**, 1428 (1994).
- ⁷ K. H. Kuit, J. R. Kirtley, W. van der Veur, C. G. Moleenaar, F. J. G. Roesthuis, A. G. P. Troeman, J. R. Clem, H. Hilgenkamp, H. Rogalla, and J. Flokstra, *Phys. Rev. B* **77**, 134504 (2008).
- ⁸ D. Y. Vodolazov, *Phys. Rev. B* **88**, 014525 (2013).
- ⁹ R. Willa, V. B. Geshkenbein, and G. Blatter, *Phys. Rev. B* **89**, 104514 (2014).
- ¹⁰ G. P. Papari, A. Glatz, F. Carillo, D. Stornaiuolo, D. Maszarotti, V. Rouco, L. Longobardi, F. Beltram, V. M. Vinokur, and F. Tafuri, *Sci. Rep.* **6**, 38677 (2016).
- ¹¹ Y.-L. Wang, A. Glatz, G. J. Kimmel, I. S. Aranson, L. R. Thoutam, Z.-L. Xiao, G. R. Berdiyrov, F. M. Peeters, G. W. Crabtree, and W.-K. Kwok, *Proc. Natl. Acad. Sci.* **114**, E10274 (2017).
- ¹² I. A. Sadovskyy, A. E. Koshelev, W.-K. Kwok, U. Welp, and A. Glatz, (2018), submitted.
- ¹³ R. Córdoba, T. I. Baturina, J. Sesé, A. Yu Mironov, J. M. De Teresa, M. R. Ibarra, D. A. Nasimov, A. K. Gutakovskii, A. V. Latyshev, I. Guillamón, H. Suderow, S. Vieira, M. R. Baklanov, J. J. Palacios, and V. M. Vinokur, *Nat. Commun.* **4**, 1437 (2013).
- ¹⁴ G. R. Berdiyrov, M. V. Milošević, M. L. Latimer, Z. L. Xiao, W. K. Kwok, and F. M. Peeters, *Phys. Rev. Lett.* **109**, 057004 (2012).
- ¹⁵ S. Tahara, S. M. Anlage, J. Halbritter, C.-B. Eom, D. K. Fork, T. H. Geballe, and M. R. Beasley, *Phys. Rev. B* **41**, 11203 (1990).
- ¹⁶ M. Benkraouda and J. R. Clem, *Phys. Rev. B* **58**, 15103 (1998).
- ¹⁷ C. P. Bean, *Phys. Rev. Lett.* **8**, 250 (1962).
- ¹⁸ C. P. Bean, *Rev. Mod. Phys.* **36**, 31 (1964).

- ¹⁹ T. Schuster, M. V. Indenbom, H. Kuhn, E. H. Brandt, and M. Konczykowski, *Phys. Rev. Lett.* **73**, 1424 (1994).
- ²⁰ A. E. Koshelev and V. M. Vinokur, *Phys. Rev. B* **64**, 134518 (2001).
- ²¹ J. K. Gregory, M. S. James, S. J. Bending, C. J. van der Beek, and M. Konczykowski, *Phys. Rev. B* **64**, 134517 (2001).
- ²² A. A. Bush, G. L. Dorofeev, V. M. Drobin, Y. D. Kuroedov, N. M. Vladimirova, and V. S. Vyatkin, *IEEE Trans. Appl. Supercond.* **12**, 1018 (2002).
- ²³ Y. N. Ovchinnikov and A. A. Varlamov, *Phys. Rev. B* **91**, 014514 (2015).
- ²⁴ G. Kimmel, A. Glatz, and I. S. Aranson, *Phys. Rev. B* **95**, 014518 (2017).
- ²⁵ I. A. Sadovskyy, A. E. Koshelev, C. L. Phillips, D. A. Karpeyev, and A. Glatz, *J. Comp. Phys.* **294**, 639 (2015).
- ²⁶ G. R. Berdiyrov, M. V. Milošević, and F. M. Peeters, *Phys. Rev. Lett.* **96**, 207001 (2006).
- ²⁷ I. A. Sadovskyy, A. E. Koshelev, A. Glatz, V. Ortalan, M. W. Rupich, and M. Leroux, *Phys. Rev. Applied* **5**, 014011 (2016).
- ²⁸ I. A. Sadovskyy, Y. Jia, M. Leroux, J. Kwon, H. Hu, L. Fang, C. Chaparro, S. Zhu, U. Welp, J.-M. Zuo, Y. Zhang, R. Nakasaki, V. Selvamanickam, G. W. Crabtree, A. E. Koshelev, A. Glatz, and W.-K. Kwok, *Adv. Mater.* **28**, 4593 (2016).
- ²⁹ I. A. Sadovskyy, Y. L. Wang, Z.-L. Xiao, W.-K. Kwok, and A. Glatz, *Phys. Rev. B* **95**, 075303 (2017).
- ³⁰ E. H. Brandt and M. Indenbom, *Phys. Rev. B* **48**, 12893 (1993).
- ³¹ L. Burlachkov, M. Konczykowski, Y. Yeshurun, and F. Holtzberg, *J. Appl. Phys.* **70**, 5759 (1991).
- ³² L. Burlachkov, *Phys. Rev. B* **47**, 8056 (1993).
- ³³ L. Burlachkov, A. E. Koshelev, and V. M. Vinokur, *Phys. Rev. B* **54**, 6750 (1996).
- ³⁴ A. E. Koshelev, I. A. Sadovskyy, C. L. Phillips, and A. Glatz, *Phys. Rev. B* **93**, 060508 (2016).
- ³⁵ R. Willa, A. E. Koshelev, I. A. Sadovskyy, and A. Glatz, *Superconductor Science and Technology* **31**, 014001 (2018).
- ³⁶ R. Willa, A. E. Koshelev, I. A. Sadovskyy, and A. Glatz, “Peak effect due to competing vortex ground states in superconductors with large inclusions,” (2018), [arXiv:1806.01986](https://arxiv.org/abs/1806.01986).
- ³⁷ G. Kimmel, I. A. Sadovskyy, and A. Glatz, *Phys. Rev. E* **96**, 013318 (2017).
- ³⁸ R. Besseling, P. H. Kes, T. Dröse, and V. M. Vinokur, *New J. Phys.* **7**, 71 (2005).